CAMBRIDGE
Cambridge University Press & Assessment
978-1-605-11515-3 — Compound Semiconductors: Thin-Film Photovoltaics, LEDs, and Smart Energy Controls Volume 1538 Edited by M. Al-Jassim, C. Heske, T. Li, M. Mastro, C. Nan, S. Niki, W. Shafarman, S. Siebentritt, Q. Wang
Excerpt
More Information

CIGS Growth

© in this web service Cambridge University Press & Assessment www.cambridge.org

CAMBRIDGE

Cambridge University Press & Assessment
978-1-605-11515-3 — Compound Semiconductors: Thin-Film Photovoltaics, LEDs, and Smart Energy Controls Volume 1538 Edited by M. Al-Jassim, C. Heske, T. Li, M. Mastro, C. Nan, S. Niki, W. Shafarman, S. Siebentritt, Q. Wang
Excerpt
More Information

Mater. Res. Soc. Symp. Proc. Vol. 1538 © 2013 Materials Research Society
DOI: 10.1557/opl.2013.997

The effect of a high temperature reaction of Cu-In-Ga metallic precursors on the formation of $Cu(In,Ga)(Se,S)_2$

Dominik M. Berg, Christopher P. Thompson, William N. Shafarman
Institute of Energy Conversion, University of Delaware, Newark, DE 19716, U.S.A.

ABSTRACT

The influence of higher processing temperatures on the formation reaction of $Cu(In,Ga)(Se,S)_2$ thin films using a three step reactive annealing process and on the device performance has been investigated. High process temperatures generally lead to the formation of larger grains, decrease the amount of void formation and their distribution at the back $Mo/Cu(In,Ga)(Se,S)_2$ interface, and lead to a much faster formation reaction that shortens the overall reaction process. However, high temperature processing also leads to a decrease in device performance. A loss in open circuit voltage and fill factor could be attributed to enhanced interface recombination processes for the samples fabricated at higher process temperatures, which itself may be caused by a lack of Na and subsequent poor passivation of interface defect states. The lack of Na resulted in a decrease in free charge carrier concentration by two orders of magnitude.

INTRODUCTION

Reactive annealing of Cu-In-Ga precursors in selenium and/or sulfur-containing atmospheres is of high interest for the commercial manufacture of $Cu(In,Ga)(Se,S)_2$ (CIGSS) absorber layers for photovoltaic devices, which have already achieved power conversion efficiencies of 17.5 % for sub-modules [1]. To date, this process has been predominantly conducted using soda-lime glass (SLG) as the substrate, which limits the reaction temperature for industrial purposes to around 520°C due to its low strain point [2]. However, photovoltaic specialty glasses are under development, which permit processing temperatures up to 650°C. Recent results for $Cu(In,Ga)Se_2$ (CIGS) co-evaporation, at temperatures between 600°C and 650°C, have demonstrated more uniform Ga-profiles, enhanced grain size, and improved open circuit voltage (Voc) and fill factor (FF) leading to increased device efficiencies [3, 4].

The reactive annealing of CIGSS has a number of commonly observed issues at the CIGSS/Mo interface, including poor adhesion, Ga accumulation, and void formation [5]. While these issues can be partly controlled at lower temperatures on SLG, increasing processing temperature offers an additional pathway to address these issues. In the present work, we examine whether higher processing temperatures enabled by alkali-containing high temperature specialty glass substrates (HTG), are also beneficial for the reactive annealing process.

EXPERIMENT

For the conducted experiments, Cu-In-Ga metallic precursors (thickness ≈ 650 nm) were prepared by sputtering multiple alternating layers of $Cu_{0.77}Ga_{0.23}$ alloy and elemental In onto Mo-coated (thickness ≈ 700 nm) HTG substrates (4” x 4”). To form CIGSS, the precursors were

© in this web service Cambridge University Press & Assessment www.cambridge.org

reacted using a three-step process in $H_2Se/Ar/H_2S$ atmospheres (see Figure 1) as described by Kim et al. [5]. This process is similar to that used by Showa Shell Sekiyu K. K., now Solar Frontier [1]. Within the scope of this work, T_1 for the H_2Se reaction step was kept at 400°C for t_1 = 40 - 50 min, while temperatures T_2 and T_3 for the Ar anneal and H_2S reaction steps, respectively, were varied between 540, 580, 600, and 650°C with t_2 = 0 - 20 min, and t_3 = 0 - 10 min. The x's in Figure 1 indicate the point where the process was stopped, following which the samples (A to I) were quickly cooled (10 – 15 °/min).

Solar cells were fabricated using a conventional glass/Mo/CIGSS/CdS/i-ZnO/ITO/Ni-Al structure [5]. The 50 nm thick CdS layer was deposited by chemical bath deposition and i-ZnO (50 nm) and ITO (150 nm) layers were deposited by RF magnetron sputtering. The Ni(50 nm)-Al(3000 nm) front contact was deposited by e-beam evaporation. The solar cells described in this study were mechanically scribed with an area of 0.4 or 1 cm^2.

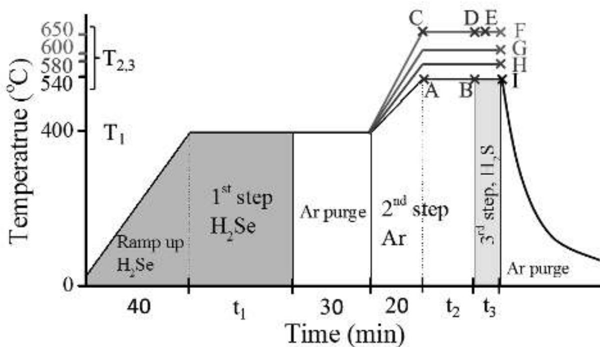

Figure 1 Temperature profile of the 3-step selenization process utilized in this study [5]. The x's indicate temperatures and times where the process was stopped and samples (A to I) were cooled.

Scanning electron microscope (SEM) analyses were performed on a JEOL JSM-7400 F and on an Amray model 1810 microscope. The latter was equipped with an Oxford Instruments PentaFET® 6900 EDX detector for compositional analysis performed with 20 kV acceleration potential. Further compositional analyses were performed using an X-ray fluorescence (XRF) system from Oxford Instruments (model X-Strata). Secondary Ion Mass Spectrometry (SIMS) depth profiles were performed by Evans Analytical Group LLC. Symmetric X-ray diffraction (XRD) scans were performed on a Philips/Norelco unit (1948 XRG, RM 190) employing a Cu X-ray source, with an acceleration potential of 35 kV and a filament compensating current of 20 mA, at a step size of 0.04° and 2 s/step integration time. Current-voltage (JV) characteristics were measured under AM 1.5 illumination at 25°C using a class A Oriel simulator. For the temperature dependent JV (JVT) measurements, a liquid nitrogen cooled Linkam cryostat (L75 920E-P) was used together with an ELH quartz halide lamp. Quantum efficiency (QE) investigations were performed using a 200 W quartz tungsten halogen projector lamp, an Oriel monochromator, a light chopper (operating at 75 Hz), and a metal halide bias lamp. To study the charge density and the width of the space charge region as a function of applied DC voltage, drive level capacitance profiling (DLCP) [6] was performed using an Agilent 4284A LCR meter and an external DC bias source.

© in this web service Cambridge University Press & Assessment www.cambridge.org

RESULTS AND DISCUSSION

Influence of high temperature on the formation reaction

In order to study the influence of high processing temperatures and times on the formation reaction of CIGSS, samples A to E were processed as shown in Figure 1 and were subsequently cooled down at the maximum rate (10 – 15 °/min). In Figure 2 (a), the results of *ex-situ* XRD analyses of samples A to E are shown. In samples A and B, processed for different times ($t_{2,A}$ = 0 min, $t_{2,B}$ = 20 min) at lower temperatures $T_{2,3}$ = 540°C, the presence of an InSe phase is observed as reported previously, at the back interface of CIGS and Mo [5]. Comparing samples A and B shows that the amount of InSe relative to CIGS does not vary over the 20 min anneal at 540°C under Ar atmosphere. At 650°C, samples C and D ($t_{2,C}$ = 0 min, $t_{2,D}$ = 20 min) still exhibit the InSe phase, but the relative amounts of this second phase are significantly smaller at t_2 = 0 min, and decreases after 20 min. In addition, the longer the film is reacted at 650°C in Ar atmosphere, the more InSe is dissolved into the CIGS film, in contrast to processing at 540°C. These results suggest that the reaction of low Ga-CIGS with Cu_9Ga_4 intermetallic, as formed in the first step at 400°C, to produce uniformly Ga-graded CIGS and the InSe secondary phase during the second anneal step [5], proceeds quicker at 650°C than 540°C. This allows a shortening of the process time for step 2. Similarly, elevated process temperatures affect the reaction rate of process step 3. Figure 2(a) shows the XRD scan of sample E ($t_{2,E}$ = 20 min, $t_{3,E}$ = 2 min). No secondary InSe phase is observed at 2 min into the third step (sample E), indicating that the InSe phase was dissolved into the CIGSS film. At the same time, the targeted average sulfur content of S/VI ≈ 0.1 could already be reached at t_3 = 2 min, as observed from EDX investigations (not shown here). This result shows the quick reaction speed at elevated temperatures (650°C) which allows a short process time for step 3 of $t_{3,650C}$ = 2 min.

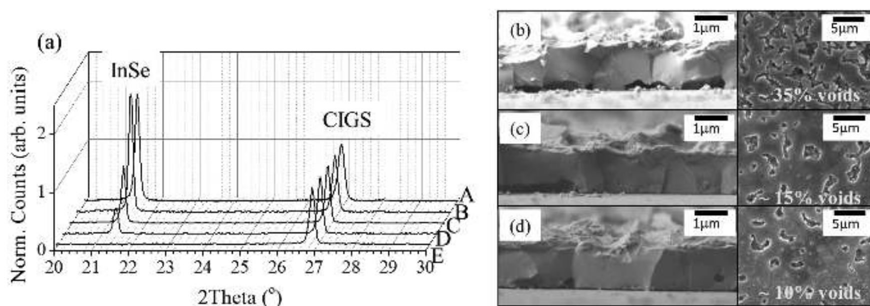

Figure 2 (a) XRD pattern obtained from samples A to E. The peaks were identified using the following JCPDS cards of the ICDD database: InSe (00-42-0919), CIGS (00-35-1102). Figures (b), (c), and (d) show SEM cross section images (left) and top view images of the back CIGSS/Mo interface after peeling (right) of samples that were fully reacted at $T_{2,3}$ = (b) 540°C, (c) 600°C, and (d) 650°C (with t_2 = 20 min, t_3 = 10 min).

Elevated reaction temperatures also have an effect on the film morphology. Figures 2(b), (c), and (d) show SEM cross-section images (left) and plan-view images of the back of the CIGSS films after peeling from the Mo (right) of samples that were fully reacted at $T_{2,3}$ = (b) 540°C, (c) 600°C, and (d) 650°C (with t_2 = 20 min, t_3 = 10 min). The cross section in Figure 2(b) looks very typical for films processed at 540°C [5]. The film consists of large columnar grains with a width of 1 - 2 µm with voids at the back interface. The back surface SEM image (Figure

© in this web service Cambridge University Press & Assessment www.cambridge.org

2(b) on the right) shows that 1 - 3 µm sized voids are distributed over ~ 35 % of the total area of the back interface. Samples processed at higher temperatures of (c) 600°C and (d) 650°C show a decrease in the total void fraction to ~ 10 % for the 650°C sample. At the same time, the lateral grain size increases by a factor of 2 to 3, leading to columnar grains with a width of 3 - 5 µm.

Influence of high reaction temperature on device performance

To study the influence of the high reaction temperature on device performance, metallic precursors were deposited on HTG and subsequently reacted in a shortened process with t_1 = 50 min and $t_2 = t_3$ = 2 min at four different reaction temperatures: $T_2 = T_3$ = 650°C (sample F), 600°C (sample G), 580°C (sample H), and 540°C (sample I). Table 1 summarizes the device performance results, composition of the absorber layers, and the activation energy, E_A, obtained from temperature dependent V_{OC} measurements (not shown here) [7]. Even though the compositions of different absorber layers are identical, the efficiency decreases systematically from 13.1 % to 3.9 % for the samples reacted at higher temperatures. The 13.1 % device obtained at 540°C is close to the results obtained on SLG, as shown in a previous work of our group, where a 14.2 % efficient device was reported [5]. The decrease in efficiency can be attributed to a drop in V_{OC} and FF, while the short circuit current (J_{SC}) is independent of the reaction temperature. At the same time, E_A, which is indicative of the dominant recombination process, decreases from E_A = 1.16 eV (the value of the CIGSS bandgap as obtained from QE measurements, see Figure 4(c)) for sample I to E_A = 0.63 eV for sample F. This result suggests that the devices reacted at higher temperatures are limited by interface recombination [8].

Table 1. Summary of device performance (after 2 min of heat treatment at 200°C in air), film composition obtained by XRF (Cu/III = Cu/(In+Ga), Ga/III = Ga/(In+Ga)) and EDX (S/VI = S/(S+Se)), and activation energies E_A of recombination processes as obtained from temperature dependent JV measurements of samples F to I. The samples were processed at different temperatures $T_{2,3}$ with t_2 = 2 min and t_3 = 2 min.

Sample	*$T_{2,3}$ (°C)*	*Eff. (%)*	*V_{OC} (mV)*	*J_{SC} (mA/cm^2)*	*FF (%)*	*Cu/III*	*Ga/III*	*S/VI*	*E_A (eV)*
F	650	3.9	240	32.1	50.6	0.94	0.26	0.11	0.63 ± 0.05
G	600	11.0	504	31.5	69.3	0.94	0.26	0.11	0.94 ± 0.05
H	580	11.9	528	32.0	70.5	0.95	0.26	0.10	0.98 ± 0.05
I	540	13.1	575	31.8	71.6	0.95	0.26	0.10	1.16 ± 0.05

To explain the JV results, SIMS depth profiles were obtained after CdS deposition. Figure 3(a) shows the composition ratios of samples F (reacted at 650°C) and I (reacted at 540°C). These show no significant differences at the surface or in the bulk. Also, an improvement in Ga homogeneity at higher temperature was not observed unlike reported elsewhere [3, 4]. This is mainly due to the already homogeneous Ga distribution that occurs at the low reaction temperature, 540°C. Figure 3(b) depicts the depth dependence of the Na concentration for samples F to I. While the glass substrates used contain Na concentrations comparable to SLG, the absorber layers reacted at higher temperatures contain progressively less Na than the film reacted at 540°C. The difference of nearly one order of magnitude explains the drop in V_{OC} by enhanced interface recombination with a lack of passivation of interface defect states [8, 9]. The cause for the difference in Na concentration for samples F to I is unresolved and a link to the enhanced grain size and, thus, lower density of grain boundaries, can only be hypothesized. Unlike Na, the amount of K throughout the depth of the films was unchanged (not shown).

© in this web service Cambridge University Press & Assessment www.cambridge.org

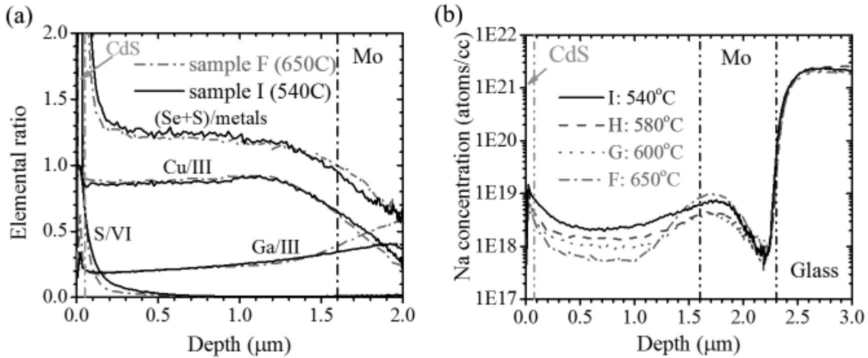

Figure 3 SIMS depth profiling of samples F to I. Graph (a) shows the elemental ratios obtained from samples F ($T_{2,3}$ = 650°C) and I ($T_{2,3}$ = 540°C). Graph (b) shows the depth profile of the Na concentration in the film, the Mo back contact, and the HTG substrate for samples F to I.

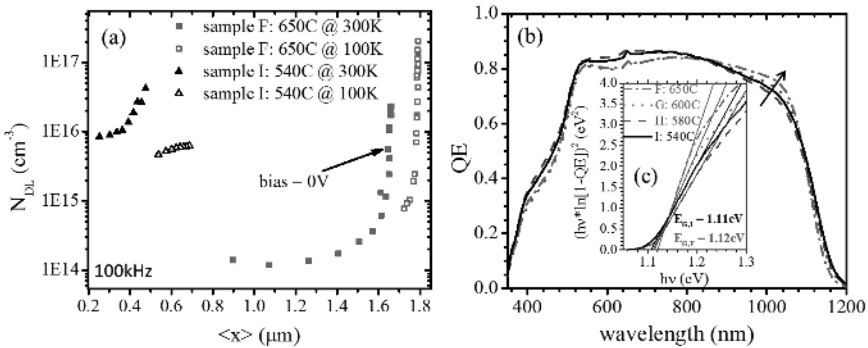

Figure 4 (a) Plot of N_{DL} over the first moment of charge response <x> as obtained from DLCP measurements performed on samples F (red/square symbols) and I (black/triangle symbols), as measured at room temperature (filled symbols) and 100 K (open symbols). (b) QE results as obtained from samples F to I at 0 V bias and in the dark. The black arrow indicates the trend for higher reaction temperatures. (c) Extrapolation of the band gap (x-axis intercept) of films F to I based on the QE results.

A difference in Na concentration of one order of magnitude in bulk CIGSS also has an influence on the free charge carrier concentration [9, 10]. In Figure 4(a), the results of DLCP measurements at room temperature (filled symbols) and 100 K (open symbols) from samples F (650°C, red symbols) and I (540°C, black symbols) are displayed. The drive level charge density (N_{DL}) at room temperature describes the sum of the defect density and the free charge carrier density N_A [6]. For sample F, N_{DL} is two orders of magnitude lower than for sample I. At T = 100 K, where $N_{DL} \approx N_A$, a similar difference of two orders of magnitude between samples F and I is suggested, although measurements on sample F in further forward bias were not possible. A decrease in N_A by two orders of magnitude, here likely related with the drop in Na

© in this web service Cambridge University Press & Assessment www.cambridge.org

concentration, can lead to a decrease in V_{OC} in CIGSS devices by itself by narrowing the quasi Fermi level splitting. Another interesting observation from Figure 4(a) is that at 0 V bias, the whole width of the absorber layer is depleted. This result correlates well with the enhanced charge carrier collection at long wavelengths in the samples reacted at higher temperatures, as shown in the QE results in Figure 4(b). Bandgap values of $E_G \approx 1.12$ eV have been observed for all samples I to F.

CONCLUSIONS

High processing temperatures were shown to result in CIGSS thin films with much larger grain size and reduced void formation at the back Mo/CIGSS interface, while the vertical compositional distribution, and especially the Ga-grading, was unchanged compared to a sample made under standard conditions. While the high temperatures lead to a faster formation reaction and, thus, shortening the overall processing time, the device performances of the samples progressively decreased as T increased from 540 to 650°C. The loss in V_{OC} and FF for the high temperature samples was concluded to be caused by enhanced interface recombination, likely originating from a lack of Na in the CIGSS material and, hence, the lack of passivation of interface defect states. Furthermore, the low Na was shown to result in a decrease in N_A.

ACKNOWLEDGMENTS

The authors would like to acknowledge John Elliot, Kevin Hart, Evan Kimberly, and Dan Ryan for their technical support, as well as Brian McCandless, Kihwan Kim, Gregory Hanket, Kevin Dobson, and Jes Larsen for fruitful discussions.

REFERENCES

[1] M. Nakamura *et al.*, "Achievement of 17.5% Efficiency with 30x30cm^2-Sized $Cu(In,Ga)(Se,S)_2$ Submodules", in *38th IEEE Photovoltaic Specialists Conference, 2012*
[2] W. Mannstadt *et al.*, “New glass substrate enabling high performance CIGS solar cells”, in *25th EU-PVSEC, 2010, p. 3516-3518*
[3] J. Haarstrich *et al.*, Sol. Energ. Mat. Sol. C. **95**, 1028-1030 (2011)
[4] M.A. Contreras *et al.*, “Improved energy conversion efficiency in wide-bandgap $Cu(In,Ga)Se_2$ solar cells”, in *37th IEEE Photovoltaic Specialists Conference, 2011*
[5] K. Kim *et al.*, J. Appl. Phys. **111**, 083710 (2012)
[6] C.E. Michelson *et al.*, Appl. Phys. Lett. **47**, 412 (1985)
[7] A.L. Fahrenbruch and R.H. Bude, “Fundamentals of Solar Cells”, *Academic press, New York, 1983, p. 236-239*
[8] C.P. Thompson *et al.*, “Temperature dependence of V_{OC} in CdTe and $Cu(InGa)(SeS)_2$-based solar cells”, in *33rd IEEE Photovoltaic Specialists Conference, 2008*
[9] P.T. Erslev *et al.*, Thin Solid Films **517**, 2277-2281 (2009)
[10] M. A. Contreras *et al.*, “On the role of Na and modifications to $Cu(In,Ga)Se_2$ absorber materials using thin-MF (M = Na, K, Cs) precursor layers”, in *26th IEEE Photovoltaic Specialists Conference, 1997*

© in this web service Cambridge University Press & Assessment www.cambridge.org

CAMBRIDGE

Cambridge University Press & Assessment
978-1-605-11515-3 — Compound Semiconductors: Thin-Film Photovoltaics, LEDs, and Smart Energy Controls Volume 1538 Edited by M. Al-Jassim, C. Heske, T. Li, M. Mastro, C. Nan, S. Niki, W. Shafarman, S. Siebentritt, Q. Wang
Excerpt
More Information

Mater. Res. Soc. Symp. Proc. Vol. 1538 © 2013 Materials Research Society
DOI: 10.1557/opl.2013.998

Analysis of NaF precursor layers during the different stages of the Cu(In,Ga)Se_2 co-evaporation process

M. Edoff[1], P.M.P. Salomé[1], A. Hultqvist[1], V. Fjällström[1]
[1]Ångström Solar Center, Department of Engineering Sciences, Uppsala University
P.O. Box 534, SE-751 21 Uppsala, Sweden

ABSTRACT

NaF precursor layers used for providing Na to Cu(In,Ga)Se_2 (CIGS) grown on Na-free substrates have been studied. The NaF layers were deposited on top of the Mo back contact prior to the CIGS co-evaporation process. The co-evaporation process was interrupted after the preheating steps, and after part of the CIGS layer was grown. Completed samples were also studied. After the preheating, the NaF layers were analyzed with X-ray Photoelectron Spectroscopy and after growing part and all of the CIGS film, the Mo/NaF/CIGS stack was characterized using transmission electron microscopy (TEM) and secondary ion mass spectrometry (SIMS). The NaF layers were found to be stable in thickness and composition during the pre-heating in selenium containing atmosphere before the CIGS process. The TEM analyses on the partly grown samples show a layer at the CIGS/Mo interface, which we interpret as a partly consumed NaF layer. This is corroborated by the SIMS analysis. In finalized samples the results are less clear, but TEM images show an increased porosity at the position of the NaF layer.

INTRODUCTION

Na is an important component in Cu(In,Ga)Se_2 (CIGS)-based solar cells. In addition to using NaF precursor layers [1] Na in-diffusion from the glass substrate can be used, but there are also other ways to include Na, as e.g. having a Na containing back contact material [2], or adding Na as a post-deposition treatment [3]. In a recent publication, modeling in combination with varying of the thickness of NaF precursor layers and thereby the Na concentration indicated that an increase of Na led to both an increased net carrier concentration as well as reduced defect density [4]. We also observed an increase of solar cell efficiency up to a certain level of Na concentration and then a saturation of the effect. In this work NaF precursor layers deposited on top of the Mo layer are studied by subsequent interruptions of the CIGS deposition process during its various stages. The Na-free substrate/Mo/NaF and Na-free substrate/Mo/NaF/CIGS stacks are analyzed with X-ray Photoelectron spectroscopy (XPS), Secondary Electron Microscopy (SEM) and Transmission Electron Microscopy (TEM) and compared to samples on soda lime glass without NaF. The objective with this study is to find out at which stages the decomposition of NaF occurs and if the NaF is stable upon heating and if it can withstand exposure to Se vapor all important input to process optimization. Samples were fabricated on soda-lime glass and on polished sintered alumina substrates. The choice of sintered alumina substrates was made in order to completely avoid the risk of Na contamination from the substrate and still get a thermal expansion coefficient which is close to that of CIGS. Soda-lime glass is the reference substrate used in our laboratory baseline process.

© in this web service Cambridge University Press & Assessment www.cambridge.org

Cambridge University Press & Assessment
978-1-605-11515-3 — Compound Semiconductors: Thin-Film Photovoltaics, LEDs, and Smart Energy Controls Volume 1538 Edited by M. Al-Jassim, C. Heske, T. Li, M. Mastro, C. Nan, S. Niki, W. Shafarman, S. Siebentritt, Q. Wang
Excerpt
More Information

EXPERIMENTAL DETAILS

The substrates were coated with a bi-layer Mo coating consisting of a thin layer (25 nm) of Mo, DC sputtered at 12 mT, followed by a 380 nm thick Mo layer sputtered at 6 mT, previously described in [5].

NaF precursor layers were deposited onto the Mo-coated substrates by thermal evaporation from a resistively heated temperature controlled source. A liner made from pyrolytic boron nitride was used to hold the NaF source material. The thicknesses of the NaF precursor layers were controlled by a quartz crystal monitor. In addition, thickness measurements were obtained from SEM cross section images. No intentional heating of the substrate was used during the NaF evaporation. After the NaF evaporation, care was taken to avoid air exposure. Samples were either stored in vacuum, in nitrogen or packed in vacuum sealed bags for transport to the analysis.

The CIGS deposition was performed by co-evaporation using two dedicated CIGS co-evaporation systems. One is a true in-line process with stable evaporation rates and moving substrates, described in [6], the other is a system with a stationary substrate arrangement, but where the evaporation rates can be controlled using a mass-spectrometer feed-back loop to mimic almost any dynamic CIGS deposition process. In the stationary co-evaporation we used a process that we believe is close to the in-line process regarding evaporation time, substrate temperature and evaporation rates. The evaporation details are illustrated in figure 1, which shows a process log from one of the runs. The left image shows the substrate and selenium source temperatures and the right image shows the evaporation rates, calculated from the mass-spectrometer signals.

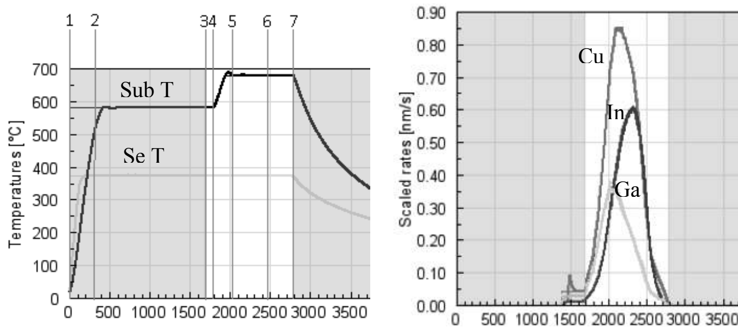

Figure 1. Process logs. Left: The heater (marked Sub T) and selenium (marked Se T) temperature profiles of the CIGS deposition process used in the stationary tool. The positions where the process was interrupted are indicated with numbers. In the gray areas the shutter is closed, while in the white area the shutter is open and the deposition of CIGS takes place. Note that the corresponding substrate temperature is lower than the heater temperature (450°C for the lower temperature region and 540 °C for the higher). Right: The evaporation rates for Cu, In and Ga.

© in this web service Cambridge University Press & Assessment www.cambridge.org

CAMBRIDGE
Cambridge University Press & Assessment
978-1-605-11515-3 — Compound Semiconductors: Thin-Film Photovoltaics, LEDs, and Smart Energy Controls Volume 1538 Edited by M. Al-Jassim, C. Heske, T. Li, M. Mastro, C. Nan, S. Niki, W. Shafarman, S. Siebentritt, Q. Wang
Excerpt
More Information

In order to closely follow the development of the NaF precursor layers during the evaporation we made several runs, where the deposition process was interrupted. The full CIGS process including the positions during the run, where the process was interrupted is shown in figure 1. As can be seen, the process was interrupted also before the shutter to the sources opened, in order to check the stability of the NaF/Mo layer stack when exposed to heat and selenium (point 1-3). For the samples interrupted during the CIGS process, we measured the compositions and thicknesses using XRF and profilometry as shown in table 1. Point 1-3, 5 and 7 are discussed more in detail in the following paragraphs. Material characterization by XPS, SIMS, SEM and TEM was made at Evans Analytical. TEM was also performed at the Angstrom laboratory.

RESULTS AND DISCUSSION

Analysis of preheated NaF precursor layers

SEM cross sections of as deposited (point 1) and pre-heated NaF (points 2 and 3) on top of Mo coated alumina substrates are shown in Figure 2. After the first heat up the thickness is unchanged, but there is a tendency of forming a more compact film with defined grains, no change is observed by SEM after heating longer at 450°C in selenium background atmosphere.

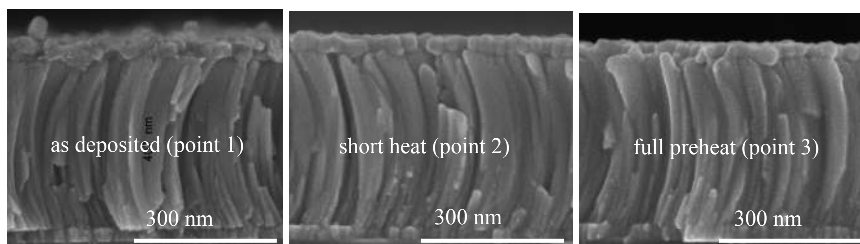

Figure 2. SEM cross section images of NaF films on top of Mo coated alumina substrates. The point notation refers to the different process interruption points shown in figure 1. The Mo grains are curved since the Mo layers are deposited in an in-line tool.

An XPS analysis was performed at point 2 and at point 3. In figure 3, the surface composition of the samples which were just heated up (point 2) of Mo/SLG and NaF/Mo/alumina are shown together with the same surfaces after the full preheating step (point 3). The NaF sample with the full heat treatment is the same as is the one shown to the right in figure 2. Although the samples were transported in evacuated air-tight bags and analyzed within one week from deposition, air exposure could not completely be avoided.

As evidenced from figure 3, there are considerable amounts of carbon and oxygen on the SLG samples, indicating that the Mo is a very reactive surface. Small, but significant amounts of Na have diffused from the SLG through the Mo and ended up on the surface. Some selenium is seen on the surface, even if the shutter that is blocking the evaporation vapors from reaching the sample is closed. This is not surprising. Selenium has a high vapor pressure and the selenium and

© in this web service Cambridge University Press & Assessment www.cambridge.org